THE ASTROPHYSICAL JOURNAL, 247:449–457, 1981 July 15

THE C IV λ1550 PROFILE IN TYPE 1 SEYFERT GALAXIES

CHI-CHAO WU[1]
Astronomy Department, Computer Sciences Corporation
AND
ALBERT BOGGESS[1] AND THEODORE R. GULL[1]
Laboratory for Astronomy and Solar Physics, NASA/Goddard Space Flight Center
Received 1980 August 7; accepted 1981 January 26

ABSTRACT

We present C IV λ1550 line profiles for the following type 1 Seyfert galaxies: NGC 5548, Mrk 509, NGC 7469, and MCG−2-58-22. We consider several possible line broadening mechanisms and the theoretical line profiles that would result. Random motion of discrete clouds is ruled out as the observed shapes are not Gaussian. A spherical ensemble of discrete clouds with steady state outflow, or inflow, would produce a logarithmic profile. This is a better fit to the data, but does not account for the highly extended wings. A spherical ensemble with ballistic outflow would produce a profile described by the first exponential integral function. Such a function, for $|\Delta\lambda| \gtrsim 5$ Å from line center, fits the observed line profile to the continuum level. While C IV profiles strongly favor the ballistic model suggested by Capriotti, Foltz, and Byard, both Mrk 509 and NGC 7469 have profiles with significant asymmetry. It is also noted that for all four galaxies, the C IV lines are at lower redshift than the Balmer lines.

Subject headings: galaxies: Seyfert — line profiles — ultraviolet: spectra

I. INTRODUCTION

The broad emission lines in Seyfert galaxies and quasars are thought to originate from discrete clouds which have large motions relative to each other. Thus, the profiles of the broad emission lines in Seyfert galaxies carry information on the kinematics and dynamics of the emitting regions. Blumenthal and Mathews (1975, 1979) proposed a spherical ensemble of discrete emitting clouds radially accelerated by radiation pressure and predicted that the lines should have a logarithmic profile. Capriotti, Foltz, and Byard (1979, 1980*a*, *b*), with detailed theoretical studies of line profiles, confirmed that the profile is logarithmic for spherical systems of clouds in steady-state radial inflow or outflow. In addition, Capriotti and his colleagues showed that clouds, which are ballistically ejected from near the central source and move outward in a force-free environment, produce an emission-line profile described by the first exponential integral function. Osterbrock (1978) proposed a model in which discrete clouds are confined to an accretion disk around the central source. The emission lines are broadened by rotation of the disk plus random motion of the clouds. The profile for Osterbrock's model is computed by Capriotti, Foltz, and Byard (1980*a*).

A very different model was proposed by Ptak and Stoner (Ptak and Stoner 1973, 1975; Stoner and Ptak 1974, 1977). They suggested that the emitting region is a stationary medium partially ionized by suprathermal particles. Photons of the broad lines are emitted by streaming excited atoms. These excited atoms are formed when an electron is transferred to a streaming ion or a streaming atom (ion) collides with a particle in the medium. Ptak and Stoner computed extensive sets of theoretical profiles for this model.

In this paper we present the observed C IV λ1550 profiles of NGC 5548, Mrk 509, NGC 7469, and MCG−2-58-22, and we compare them with Gaussian, logarithmic, and the first exponential integral profiles. We chose the C IV line because its neighboring lines, such as N IV] λ1486, [Ne V] λ1575, and [Ne IV] λ1602, are all very weak and do not contaminate the C IV profile significantly. Moreover, compared to Lyα, C III] λ1909, and Mg II λ2800, C IV λ1550 is relatively free of instrumental effects.

II. OBSERVATIONS

Observations were made with the short wavelength prime (SWP) camera on board the *International Ultraviolet Explorer* (*IUE*) satellite. Spectral coverage is from

[1]Guest Investigator of the *IUE* Observatory, operated by the Goddard Space Flight Center, National Aeronautics and Space Administration.

1150 Å to 2000 Å and, in low-dispersion mode, the spectral resolution is 5 Å. Descriptions of the *IUE* scientific instruments and their performance are given in Boggess *et al.* (1978*a*, *b*).

All spectra used in this investigation were broadened (equivalent to trailed) to increase the signal-to-noise ratio. A broadened spectrum can be obtained by taking three separate spectra through the $10'' \times 20''$ large aperture. The broadening is accomplished by placing the object at three different locations in the large aperture along the *X*-axis of the fine error sensor (FES2). The three locations, separated by 4″, lie perpendicular to the spectrograph dispersion direction, and the wavelength smearing is expected to be negligible. The three spectra merge smoothly without significant overlaps or gaps. The advantage this pseudo-trail technique has over actual trailing is that, during each exposure, the spacecraft can be stabilized by locking it to a guide star. Whereas the *IUE* is capable of obtaining high quality trailed spectra for brighter objects, even the brightest Seyfert nuclei may require several hours to obtain a sufficiently widened spectrum. The required trail rate is too low to be reliably performed by the on-board attitude control system and, without tracking on a guide star, there will be some drift along the dispersion direction.

The SWP images were processed with the extended source reduction schemes by the image processing staff at the *IUE* Observatory. Since all the images were taken in 1979 December, the correct intensity transfer function (ITF) was used in the reduction. The absolute calibration of Bohlin *et al.* (1980) was adopted to establish the absolute flux levels of the spectra. The calibrated C IV λ1550 profiles are given in Figure 1. No reddening correction has been applied to the observed fluxes. As shown by Bless and Savage (1972) and Wu, Gilra, and van Duinen (1980), the galactic extinction curves are relatively flat around the 1550–1800 Å region. From the average extinction curve of Code *et al.* (1976), the difference in reddening over 100 Å is 0.2 mag per unit $E(B-V)$ between 1500 and 1650 Å. Typically, $E(B-V)$ is ~ 0.1 for these objects. With the half-width at zero intensity of ~ 50 Å, the difference in reddening between the line center and the far wings is about 0.01 mag. Therefore, reddening by the dust outside the emitting region cannot modify the line profile significantly.

A brief description for each individual spectrum is given below:

NGC 5548 (Fig. 1*a*).—A strong absorption feature severely contaminates the blue portion of the line peak. We will use only the red portion for our analysis. This C IV self-absorption is strongest in NGC 4151 (Boksenberg *et al.* 1978) and is weakly present in several other objects (see below). In the rest frame corresponding to the optical lines (see Weedman 1977), the weak feature at 1603 Å is [Ne V] λ1575. Similarly, the broad feature around 1614 Å is tentatively identified as Si I multiplets 37, 38, 36, and 34 which extend from 1584 Å to 1594 Å.

Mrk 509 (Fig. 1*b*).—In the rest frame defined by the redshift of the C IV line, the weak feature centered at 1575 Å is identified as Si II λ1526. The sharp feature at 1556 Å is a "radiation hit," caused by a high-energy particle interacting with the SEC vidicon camera. Such radiation hits contaminate *IUE* spectral images and are identifiable as black dots, smudges, or streaks on photographic reproductions of the raw image. (These photographic image reproductions are known as "photowrites" and are routinely checked for evidence that radiation hits may have contaminated the recorded spectra.) Near the peak intensity of the C IV line, the profile is slightly weaker on the long wavelength side. Two high-dispersion spectra (~ 0.2 Å resolution) show that C IV λλ1548.2 and 1550.8 absorptions in the rest frame of Mrk 509 and Fe II λ1608.5 absorption in the rest frame of our own Galaxy (York *et al.* 1981) are the cause of the slight asymmetry near the peak intensity (the asymmetry of the whole profile is discussed in § IV*b*).

NGC 7469 (Fig. 1*c*).—Self-absorption affects the blue side of the line center. The features at 1551 Å and 1612 Å can be identified, respectively, as Si II λ1526 and the Si I multiplets which cover 1584–1594 Å. Using the redshift defined by C IV λ1550, the weak line at 1595 Å is identified as [Ne V] λ1575. The strong feature shortward of 1545 Å is a radiation hit, confirmed in the photowrite image as a small black dot plus a weak smudge adjacent to the spectrum.

MCG−2-58-22 (Fig. 1*d*).—The width of this line is enormous (note that the wavelength scale for this plot is twice that used for the others). The center of this line is affected by self-absorption. The crosses near 1660 Å indicate the region affected by a reseau mark (blind spot) on the camera faceplate. With the redshift given by Ward *et al.* (1978), the features at 1663, 1680, and 1715 Å are the Si I λλ1584–1594 multiplets, [Ne IV] λ1602, and He II λ1640, respectively. [Ne V] λ1575 may have been lost in the reseau mark. The strong feature at 1687 Å is a radiation hit. The line at 1595 Å can be Si II λ1526 if the redshift of C IV λ1550 is used. The feature at 1580 Å may be real, but no line is known at its rest wavelength (1509 Å).

The uncertainty in measured wavelengths of properly exposed, sharp emission lines in SWP low-dispersion spectra is 2.5 Å (Harvel, Turnrose, and Bohlin 1979). However, the lines discussed above are very weak; even small amounts of noise can significantly change their apparent wavelengths. Therefore, the redshift differences among these lines, whether they shift with the C IV line or the optical lines, should be considered as tentative. The redshift of C IV λ1550 is discussed in § IV*c*.

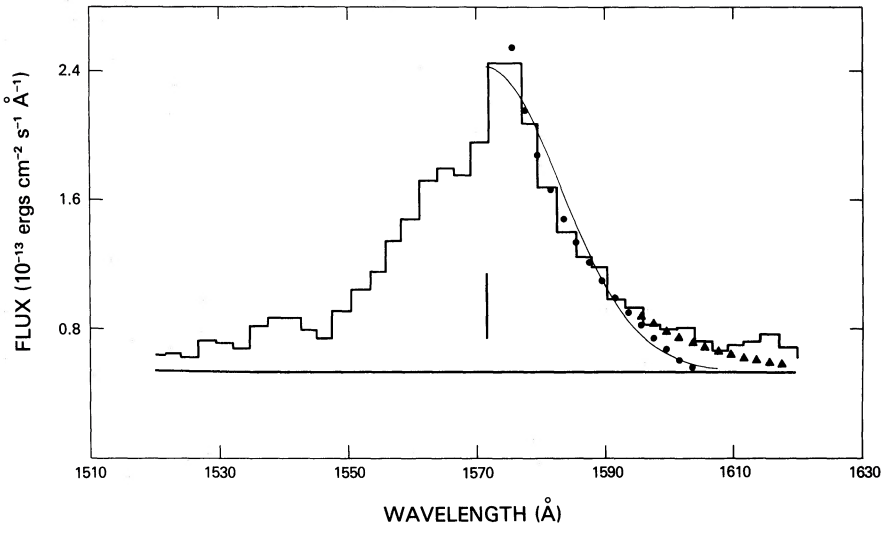

FIG. 1*a*

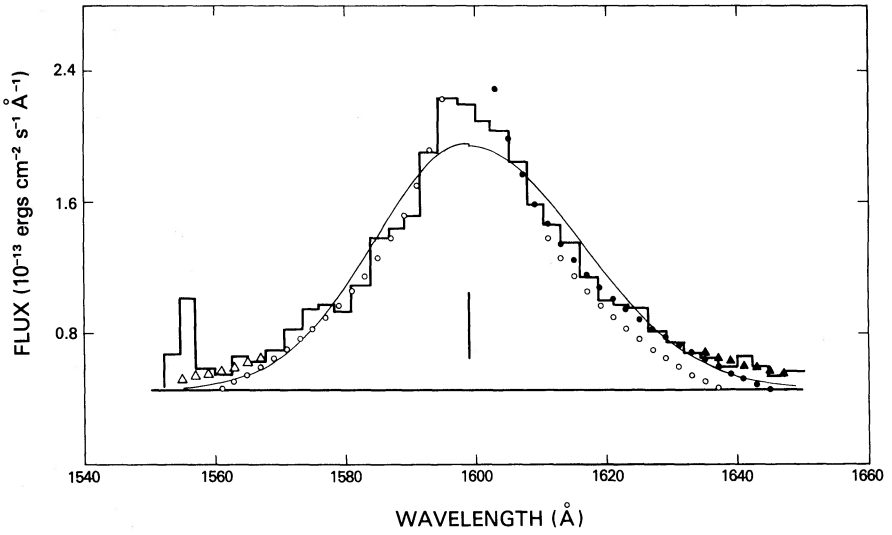

FIG. 1*b*

FIG. 1.—The C IV λ1550 profile of type 1 Seyfert galaxies: (*a*) NGC 5548, (*b*) Mrk 509, (*c*) NGC 7469, and (*d*) MCG−2-58-22. The stepped profile is the observed C IV emission line. The horizontal and vertical straight lines are the adopted continuum level and line center, respectively. The thin smooth curves are the Gaussian profiles. The circles and triangles represent the logarithmic and first exponential integral profiles, respectively, with open symbols for the short-wavelength side and solid symbols for the long-wavelength side. The first exponential integral profiles are plotted only in the far wings because, for regions closer to the center, the first exponential integral profiles are essentially the same as the logarithmic profiles. For Mrk 509 and NGC 7469, the short side of the logarithmic profile is reflected on the long side to show the asymmetry of the emission line.

III. ANALYSIS

a) *Establishing the Continuum Level*

For Seyfert galaxies, the 1200–1800 Å spectral region is rich in emission lines. From our widened spectra of NGC 4151 and the four type 1 Seyferts discussed at present, only four continuum windows can be identified. These windows have the following central wavelengths and full widths (in parentheses): 1345 Å (50 Å), 1445 Å (50 Å), 1700 Å (30 Å), and 1790 Å (60 Å). The windows are sufficiently far from the line to avoid contamination by its broad wings. Sometimes one or even two of these windows can be contaminated by a reseau mark or a radiation hit. In this investigation, the continuum level for C IV λ1550 was established by these four windows. No elaborate fitting to different continuum shapes is

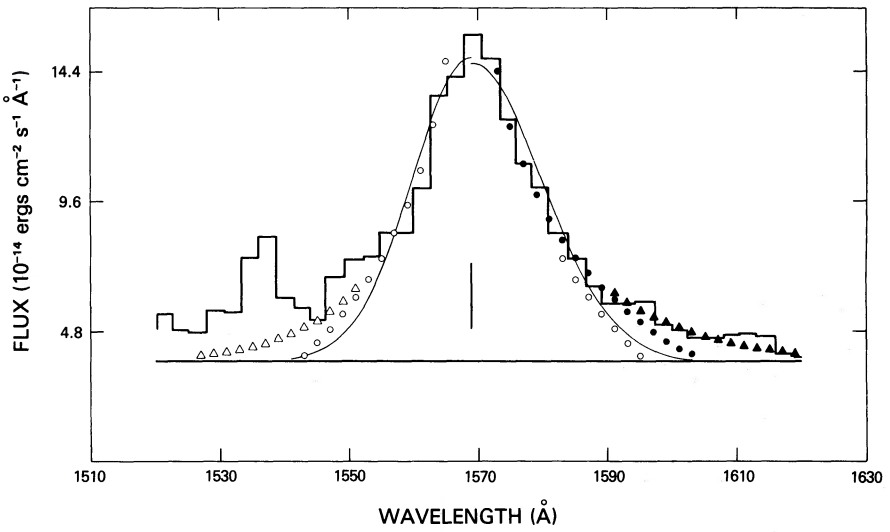

FIG. 1*c*

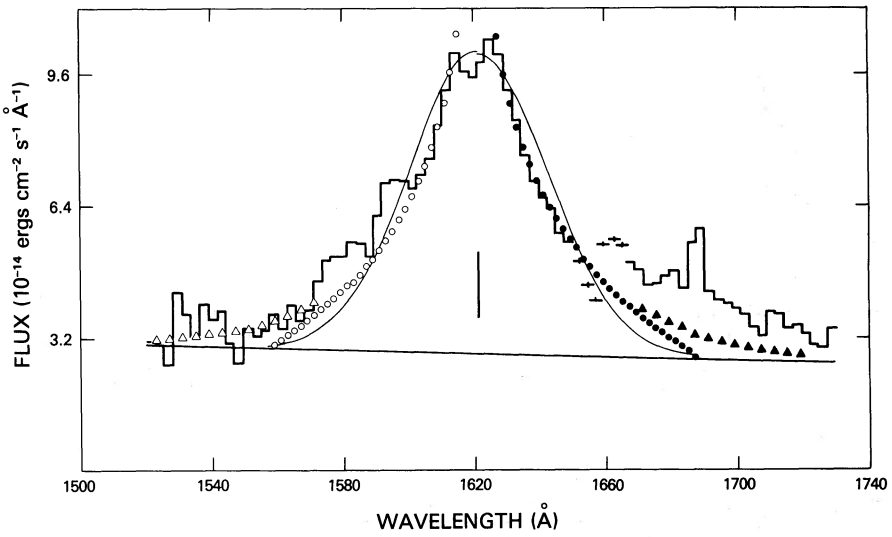

FIG. 1*d*

justified. In a related paper (Wu, Boggess, and Gull 1980), we measured Lyα fluxes for 14 type 1 Seyferts and quasars, including the four objects discussed here. In all cases, a linear relationship adequately fitted the continuum windows.

b) Establishing the Line Center

Once the continuum level was established by linear fit, we then examined the line profile in the range of 70–90% of the peak intensity. In this there are no significant asymmetries, but the 90–100% peak intensity portion of the line profile is contaminated by unresolved absorption lines (see § II). We chose line center to be the wavelength midway between the 70–90% portions of the line profile. However, in the case of NGC 5548, the short wavelength side of the C IV line is strongly absorbed in this intensity range. We chose its line center as midway between the 50% peak intensity points.

This procedure to establish line center implicitly requires either that the emission from the narrow-line region (NLR) contributes symmetrically to the broad-line profile or that it is weak and affects only the top 10% of the line. We can estimate the strength of the narrow component from the measured fluxes of [O III] λ5007, since they both arise from the NLR. NGC 1068 is the only type 2 Seyfert for which both the C IV and

[O III] fluxes are available. The observed $f_{1550n}/f_{5007}=0.28$ (Boksenberg *et al.* 1978; Koski 1978); *n* indicates that it is a narrow line. According to Neugebauer *et al.* (1980), $E(B-V)=0.4$ is needed in order to make the observed emission-line ratios agree with the values predicted by photoionization models. The extinction curve of Code *et al.* (1976) gives $E(1550-5007)/E(B-V)=4.68$. Correcting for $E(B-V)=0.4$, $f_{1550n}/f_{5007}=1.57$. The f_{5007} of NGC 5548, Mrk 509, and NGC 7469 can be derived from the measurements of Osterbrock (1977) together with the total Hβ fluxes compiled by Wu, Boggess, and Gull (1980). The resulting values of f_{5007} are, respectively, 10.3, 5.5, and 10.0×10^{-13} ergs cm^{-2} s^{-1}. Then the $f_{1550n}=16.2$, 8.6, and 15.7×10^{-13} ergs cm^{-2} s^{-1}, respectively. Table 1 gives the observed fluxes of the C IV line. After correcting for the reddening estimated from the 2200 Å feature (see § IV*b*), $f_{1550}=12.2$, 8.9, and 20.5×10^{-12} ergs cm^{-2} s^{-1}, respectively, for the three galaxies. Consequently, $f_{1550n}/f_{1550}=13\%$, 10%, and 8%, respectively, for NGC 5548, Mrk 509, and NGC 7469.

As shown above, if the physical conditions in the NLR of type 1 Seyferts are the same as those of NGC 1068, $f_{1550n}/f_{1550}\sim0.1$. But in Mrk 509 this ratio must be significantly lower than 0.1, since two high-dispersion spectra with 0.2 Å resolution show no noticeable narrow component (York *et al.* 1981). Furthermore, the four galaxies we consider here all have broad lines. At the 70–90% flux levels, their C IV lines have a full width of ~15 Å, or 3 resolution elements. A narrow component having 10% of the flux of the broad component should be clearly resolved. As shown in Figure 1, the narrow component is not detectable. From this evidence, we conclude that the narrow component of the C IV line is negligible in these four galaxies and does not introduce any appreciable uncertainty in our determination of the line centers of the broad component.

There are several possibilities why the earlier estimate (that the narrow component might be 10% of the flux of the broad component) is too high: (1) the reddening correction for the C IV line of NGC 1068 is too large; (2) the NLR of NGC 1068 has higher excitation and is not representative of the NLR of type 1 and other type 2 Seyferts (e.g., the FWHM of the lines in NGC 1068 is 1200 km s^{-1} rather than the typical 500 km s^{-1} for other NLRs); (3) the four galaxies have very dominant BLRs ($f_{5007}/f_{H\beta}\sim0.5$) which may have absorbed most of the high-energy photons so that not enough photons leak out to produce the high excitation lines like C IV λ1550 in the NLR.

c) Profile Fitting

Theoretical profiles were fitted independently to the red and blue sides of the observed profile. Two points were chosen on the hand-drawn smooth curves to establish the constants A and B of the following theoretical profiles:

Gaussian: $$F_\lambda = A\,e^{-(\Delta\lambda)^2/B}, \quad (1)$$

Logarithmic: $$F_\lambda = A\ln|\Delta\lambda| + B, \quad (2)$$

First Exponential Integral: $$F_\lambda = AE_1\left[B(\Delta\lambda)^2\right] = AE_1(x). \quad (3)$$

F_λ is given in ergs cm^{-2} s^{-1} Å^{-1}, and $\Delta\lambda$ is given in Å from the line center. The derivations of equations (2) and (3) are presented by Capriotti, Foltz, and Byard (1980*a*). Values for A and B can be obtained using the two points selected from the observed profile for equations (1) and (2). For equation (3), the numerical value of $E_1(x)$ is given in Gautschi and Cahill (1965), so values of A and B are obtained by iteration. The computed profiles are superposed on the calibrated profiles in Figure 1.

IV. DISCUSSION

a) Comparison between Observed and Computed Profiles

i) *Gaussian Profile*

Gaussian profiles are plotted in Figure 1 as thin, smooth curves. Between the two points selected for fitting the theoretical and observed profile, the Gaussian profile is significantly broader than the observed line. Toward the lower portion of the line and out in the wings, the computed Gaussian profile lies well below the observed fluxes. For the four Seyferts considered in this investigation, the Gaussian profile fails badly in fitting the observations. This failure rules out models which call for discrete clouds in random motion as the main line-broadening mechanism.

ii) *Logarithmic Profile*

Logarithmic profiles are plotted in Figure 1 as filled circles for the long wavelength side of the line and open circles for the short wavelength side. The logarithmic profile fits the observed line exactly in the region from 90% to 20% of the peak intensity. Near the line center ($|\Delta\lambda|\lesssim5$ Å), the logarithmic profile diverges. In the wings, its prediction falls below the observed fluxes. The divergence at the line center for the logarithmic profile is a mathematical feature which must be physically incorrect. Blumenthal and Mathews (1975) suggested that when the discrete clouds are formed near the central source, they acquire an initial velocity of several hundred kilometers per second. These clouds, in random or radial motion, would produce a flat top near the line center.

TABLE 1

PARAMETERS ASSOCIATED WITH THE C IV λ1550 PROFILE

Parameter	NGC 5548	Mrk 509	NGC 7469	MCG–2-58-22
Line center	1571.5	1599.0	1569.0	1621.0
Continuum at line center[a] (10^{-14} ergs cm^{-2} s^{-1} Å^{-1})	5.40	4.60	3.72	2.82
Redshift (z):				
Optical	0.01663	0.03550	0.01673	0.04793
C IV λ1550	0.01420	0.03195	0.01258	0.04614
Half-width at half-maximum (Å):				
Red	11.2	14.0	10.2	19.2
Blue	11.2	12.5	9.4	18.9
Half-width at $1/e$ of maximum (Å):				
Red	14.7	19.4	13.9	28.2
Blue	14.4	17.0	12.5	27.0
Half-width at zero intensity (Å):				
Red	49	58	57	112
Blue	...	50	47	109
Integrated flux[b] (10^{-12} ergs cm^{-2} s^{-1}):				
Red	2.87	3.21	1.71	2.10
Blue	...	2.88	1.42	2.04
Total equivalent width (Å)	106[c]	132	84	147
Constants for Gaussian profile:				
Red: A	1.88	1.48	1.10	0.73
B	266.39	579.09	233.06	905.64
Blue: A	...	1.51	1.12	0.73
B	...	409.55	164.93	963.49
Constants for logarithmic profile:				
Red: A	−0.96	−0.75	−0.49	−0.32
B	3.33	2.87	1.75	1.34
Blue: A	...	−0.79	−0.58	−0.33
B	...	2.88	1.91	1.35
Constants for first exponential integral profile:				
Red: A	0.53	0.42	0.26	0.17
B (10^{-4})	7.55	4.00	5.58	1.56
Blue: A	...	0.45	0.31	0.17
B (10^{-4})	...	6.10	9.76	1.72

[a] The continuum level is approximately flat for all objects except MCG–2-58-22 which has $f_\lambda = 3.04 \times 10^{-14}$ ergs cm^{-2} s^{-1} Å^{-1} at the observed wavelength of 1525 Å and $f_\lambda = 2.64 \times 10^{-14}$ ergs cm^{-2} s^{-1} Å^{-1} at 1710 Å.

[b] Adopting the first exponential integral profiles for the far wings.

[c] Assuming the blue side has the same integrated flux as the red side.

For a spherical ensemble of discrete emitting clouds, Blumenthal and Mathews (1975, 1979) found that a logarithmic profile will result from clouds radially accelerated by radiation pressure. Capriotti, Foltz, and Byard (1980*a*) considered various possible dynamical conditions in the broad-line region (BLR). They concluded that discrete clouds which are spherically distributed, and which have a steady-state radial motion with their velocity and acceleration vectors pointing either toward or away from the central ionizing source, would produce a logarithmic profile. The excellent agreement between the logarithmic and the observed line profiles, from the 90% to the 20% level of the peak intensity, indicates that the basic features of the model—spherical distribution and radial motion of the emitters—are probably correct. The failure of the logarithmic profile to fit the observed wings of the lines is probably attributable to the types of motion considered. As will be discussed in the next subsection, a nonsteady-state outflow will produce a profile which can match the observed line from the 90% level of the peak intensity to the continuum level in the far wings.

Osterbrock's (1978) model of discrete clouds confined to an accretion disk can produce many of the observed features of Seyfert galaxies. In this model, the clouds participate in the rotation of the disk and have turbulent

motion relative to each other. However, as pointed out by Capriotti, Foltz, and Byard (1980*a*), the theoretical profile based upon the disk model deviates significantly from the logarithmic profile and does not fit the observed emission-line profiles.

In the particle streaming model of Ptak and Stoner (1973, 1975; Stoner and Ptak 1974, 1977), the lines are broadened by the relative motions of the individual emitting ions. In this model, the emitters also have a spherically symmetric distribution and possess radially outward motion. The resulting profile should be quite similar to the logarithmic profile, if the medium is relatively transparent to line photons. The computed profiles provide a reasonably good fit with the observations (see, e.g., Stoner, Ptak, and Ellis 1974). In addition, this model provides quantitative predictions on the relative widths of lines according to the ionization potentials of the emitting ions. However, Osterbrock and Koski (1976) and Boksenberg *et al.* (1975) already have pointed out that the widths of He I, He II, and H I lines are not consistent with the model predictions. We will defer the discussion of the Ptak-Stoner model to a later paper, when we compare the profiles of the lines of hydrogen, C IV, C III], and Mg II.

iii) *First Exponential Integral Profile*

The first exponential integral function in equation (3) can be expanded as $E_1(x)=-\gamma-\ln x-\Sigma_{n=1}^{\infty}(-1)^n x^n/nn!$ (Gautschi and Cahill 1965), where $\gamma=0.577$, is the Euler constant. As pointed out by Capriotti, Foltz, and Byard (1980*a*), the first exponential integral function becomes a logarithmic function at small x (small $|\Delta\lambda|$). For large x, which is appropriate for the wings of the emission line, the first exponential integral profile predicts higher fluxes than the logarithmic profile. In Figure 1, the first exponential integral profiles are indicated by triangles for large $|\Delta\lambda|$ from the line center. For smaller $|\Delta\lambda|$, they are essentially the same as the logarithmic profile and, therefore, not plotted. As shown in Figure 1, an excellent fit is achieved by the first exponential integral profile from 90% of the peak intensity to the continuum level in the far wings. The excess emission in the short-wavelength wing of NGC 7469 is due to the radiation hits caused by high-energy particles impinging on the camera. In the long-wavelength wing of MCG−2-58-22, excess flux comes from a combination of neighboring lines and a radiation hit.

From the study of Capriotti, Foltz, and Byard (1980*a*), the first exponential integral profile is produced by spherically distributed discrete clouds which are ballistically ejected from near the central source. An impulsive force provides the clouds with their initial velocity and, subsequently, the clouds move in a force-free environment. The initial velocities of the clouds are directed radially outward with speeds which are assumed to have a Maxwellian distribution. Except for the mathematical divergence near the line center, the first exponential integral profile fits the C IV λ1550 from $|\Delta\lambda|\sim 5$ Å to $|\Delta\lambda|\sim 50$–100 Å. This excellent agreement between model predictions and observations greatly strengthens the ballistic model as a realistic representation of the true dynamical condition in the BLR of active galaxies. Of course, the origin of the discrete clouds and the mechanism by which the impulsive force imparts momentum to the clouds still remain to be understood.

Following the formalism of Capriotti, Foltz, and Byard (1980*a*), the constant B in equation (3) can be expressed as

$$B=\frac{c^2}{(\lambda_0 V_D)^2}, \tag{4}$$

where λ_0 is the rest wavelength of the emission line in Å, c is the velocity of light, and V_D is the most probable speed of the Maxwellian distribution. V_D and c have the same units. B is given in Table 1. Adopting the B value for the long wavelength side of the profiles, which is less affected by attenuation, the most probable speed for the clouds is 7.0×10^3, 9.7×10^3, 8.2×10^3, and 1.6×10^4 km s^{-1}, respectively, in NGC 5548, Mrk 509, NGC 7469, and MCG−2-58-22. The enormous speed of the clouds in MCG−2-58-22 is of course reflected in the equally enormous width of the C IV line. The derivation of the number of clouds in the BLR of each galaxy will require detailed computation and is beyond the scope of this investigation.

b) *Asymmetry*

The half-widths at the half, e^{-1}, and zero intensity levels of the first exponential integral profile are given in Table 1, separately for the long and short wavelength sides. NGC 5548 and MCG−2-58-22 have reasonably symmetric C IV λ1550 lines, but for Mrk 509 and NGC 7469 the long wavelength side is significantly broader. This is also shown in Figures 1*b* and 1*c* in which the short side of the logarithmic profile (open circle) is reflected on the long side. This is consistent with the asymmetry found by Osterbrock (1977) for the hydrogen Balmer lines. The fluxes for the long and short wavelength sides of the line and the total equivalent widths are also given in Table 1. The fluxes were measured by following the observed (stepped) profile to the point where the first exponential integral begins to deviate from the logarithmic profile. From that point on, the smooth first exponential integral profile was followed to the continuum level in the far wings.

Opacity from dust and/or resonance scattering can produce asymmetry in emission lines. The opacity can exist in the region of the cloud which is facing away from the central ionizing source. Capriotti, Foltz, and Byard (1979, 1980*b*) suggested dust as the opacity

source, while Ferland, Netzer, and Shields (1979) considered self-absorption. As these authors and Blumenthal and Mathews (1979) pointed out, the photons can preferentially escape from the side facing the central source. When the clouds are moving radially outward, the blueshifted photons will be suppressed. This is in agreement with the observed asymmetry of the H I Balmer lines and C IV λ1550.

Of the four objects, NGC 5548 has the strongest C IV absorption, but its profile is rather symmetric. From our preliminary study of the 2200 Å dust absorption feature for these objects, NGC 7469 has $E(B-V) \sim 0.25$, NGC 5548 and MCG−2-58-22 have $E(B-V) \sim 0.1$, and Mrk 509 has $E(B-V) \sim 0.05$. NGC 7469 and Mrk 509 have the highest and lowest $E(B-V)$, respectively, and yet they have the most asymmetric profiles. The location(s) of the dust and the absorbing gas is also uncertain. They may be in the discrete clouds, the intercloud medium, or in areas totally outside the BLR. If dust plays a major role, one can expect the asymmetry to increase for lines at shorter wavelengths, e.g., C IV λ1550 should be more asymmetric than Hβ. If self-absorption is the main opacity source, then the asymmetry will depend on the atomic absorption optical depth of the individual lines. Our scenario for the BLR (see § III*d* below) favors the latter.

If the opacity source exists in the intercloud medium, the photons from the far side of the BLR will be suppressed. In order to have more flux on the red side, the clouds will have an inward motion. If the motion is indeed inward, gravitational redshift may contribute additional asymmetry in favor of the longer wavelengths (Anderson 1979, 1980). The inflow model cannot be conclusively ruled out. Capriotti, Foltz, and Byard (1980*a*) provide several arguments in favor of the ballistic model and, as we pointed out earlier, the excellent agreement between the first exponential integral profile and the observed C IV λ1550 profile of four objects is strong evidence in support of the ballistic model.

c) *Redshift*

The line center obtained in § III is used to calculate the redshift of C IV λ1550. The results are given in Table 1. The redshifts given in Weedman (1977) and Ward *et al.* (1978) are obtained from lines in the optical region, such as Balmer lines; these are also given in Table 1. The C IV λ1550 redshift is consistently smaller. While the wavelength uncertainty in *IUE* SWP images is about 2.5 Å (Harvel, Turnrose, and Bohlin 1979), the difference in wavelength shifts between the C IV and optical lines is 3–6 Å with the asymmetric lines having the larger values. The centroids of the asymmetric lines of Mrk 509 and NGC 7469 are about 1 Å longer than the line centers given in Table 1 and cannot be the cause of the difference. Admittedly, the difference is not large when one considers the probable error of 2.5 Å, but in all four cases the C IV redshift is smaller than the redshift obtained from the optical lines. The difference is probably real, and there is stratification in the line-formation regions.

d) *A Plausible Scenario*

In this investigation we have found: (1) C IV λ1550 has a profile best fitted by a first exponential integral function; (2) the C IV line of some objects shows significant asymmetry with excess emission in the red side; (3) C IV λ1550 has a slightly lower redshift than the Balmer lines; and (4) from our own work and that of Oke and Zimmerman (1979), C IV λ1550 is broader than Lyα for some objects. When we compare the FWHM and FWZI of the C IV line (the sum of the half-widths in Table 1) and those of Hβ, as given by Osterbrock (1977) and Ward *et al.* (1978), the expansion velocity of the discrete clouds derived from the C IV line is higher by 10%, 20%, 60%, and 90%, respectively, for NGC 5548, Mrk 509, NGC 7469, and MCG−2-58-22. In NGC 7469 and MCG−2-58-22, the large discrepancy between the FWZI of C IV λ1550 and Hβ may not be real. As shown in Figure 1 and Table 1, these two objects have the largest ratio of FWZI/FWHM. The broad but weak wings of their first exponential integral profiles take the slowest asymptotic approach to zero intensity. It is likely that less extensive wings were adopted for Hβ. In addition, Osterbrock (1977), Elvis *et al.* (1978), and Wu *et al.* (1979) found that the higher luminosity objects have broader lines.

A plausible scenario can be constructed to explain the observed properties of emission lines. Discrete clouds are formed near the central source with a random or radial velocity of several hundred kilometers per second. This will produce a flat top near the line center. Within a short time (for an impulsive force to be effective) the clouds are accelerated to an equilibrium radial velocity which has a Maxwellian distribution whose most probable speed is higher for more luminous objects. The clouds have a spherical distribution and their radially outward motion may experience further slight acceleration or deceleration. If it is deceleration, the broader C IV λ1550 lines are formed closer to the central source than the H I lines. The clouds can be optically thick to line radiation and emit anisotropically by having the photons escape preferentially toward the central ionizing source. This leads to line asymmetry. The Balmer lines have higher optical depth and, therefore, are more biased by clouds on the far side of the central source. Consequently, the Balmer lines should show higher asymmetry and redshift.

It is a pleasure to thank Dr. Eugene Capriotti for some illuminating discussions. We also wish to thank Joy Heckathorn for her help in data reduction, and Francis Schiffer for allowing us to use his data reduction system. This work was supported in part by *IUE* research contract NAS5-25774.

REFERENCES

Anderson, K. S. 1979, *Bull. AAS*, **11**, 638.
_____. 1980, preprint.
Bless, R. C., and Savage, B. D. 1972, *Ap. J.*, **171**, 293.
Blumenthal, G. R., and Mathews, W. G. 1975, *Ap. J.*, **198**, 517.
_____. 1979, *Ap. J.*, **233**, 479.
Boggess, A. *et al.* 1978*a*, *Nature*, **275**, 372.
_____. 1978*b*, *Nature*, **275**, 377.
Bohlin, R. C., Holm, A. V., Savage, B. D., Snijders, M. A. J., and Sparks, W. M. 1980, *Astr. Ap*, **85**, 1.
Boksenberg, A., Shortridge, K., Allen, D. A., Fosbury, R. A. E., Penston, M. V., and Savage, A. 1975, *M.N.R.A.S.*, **173**, 381.
Boksenberg, A. *et al.* 1978, *Nature*, **275**, 404.
Capriotti, E., Foltz, C., and Byard, P. 1979, *Ap. J.*, **230**, 681.
_____. 1980*a*, *Ap. J.*, **241**, 903.
_____. 1980*b*, preprint.
Code, A. D., Davis, J., Bless, R. C., and Hanbury Brown, R. 1976, *Ap. J.*, **203**, 417.
Elvis, M., Maccacaro, T., Wilson, A. S., Ward, M. J., Penston, M., Fosbury, R. A. E., and Perola, G. C. 1978, *M.N.R.A.S.*, **183**, 1.
Ferland, G. J., Netzer, H., and Shields, G. A. 1979, *Ap. J.*, **232**, 382.
Gautschi, W., and Cahill, W. F. 1965, *Handbook of Mathematical Functions*, ed. M. Abramowitz and I. A. Stegun (New York: Dover), p. 277.
Harvel, C. A., Turnrose, B. E., and Bohlin, R. C. 1979, *IUE Newsletter No.* 5, ed. Y. Kondo (Greenbelt: Goddard Space Flight Center).
Koski, A. T. 1978, *Ap. J.*, **223**, 56.
Neugebauer, G. *et al.* 1980, *Ap. J.*, **238**, 502.
Oke, J. B., and Zimmerman, B. 1979, *Ap. J.* (*Letters*), **231**, L13.
Osterbrock, D. E. 1977, *Ap. J.*, **215**, 733.
_____. 1978, *Astronomical Papers Dedicated to Bergt Stromgren*, ed. A. Reitz and T. Andersen (Copenhagen: Copenhagen University Observatory), p. 299.
Osterbrock, D. E., and Koski, A. T. 1976, *M.N.R.A.S.*, **176**, 61P.
Ptak, R., and Stoner, R. E. 1973, *Ap. J.*, **185**, 121.
_____. 1975, *Ap. J.*, **200**, 558.
Stoner, R. E., and Ptak, R. 1974, *Astr. Ap.*, **35**, 191.
_____. 1977, *Ap. J.*, **214**, 653.
Stoner, R. E., Ptak, R., and Ellis, D. 1974, *Ap. J.*, **191**, 291.
Ward, M. J., Wilson, A. S., Penston, M. V., Elvis, M., Maccacaro, T., and Tritton, K. P. 1978, *Ap. J.*, **223**, 788.
Weedman, D. W. 1977, *Ann. Rev. Astr. Ap.*, **15**, 69.
Wu, C.-C., Boggess, A., and Gull, T. R. 1980, *Ap. J.*, **242**, 14.
Wu, C.-C., Boggess, A., Gull, T. R., Mushotsky, R. F., Boldt, E. A., Holt, S. S., and Serlemitsos, P. J. 1979, *Proceedings of a Symposium*: *The First Year of IUE*, ed. A. Willis (London: University College London), p. 157.
Wu, C.-C., Gilra, D. P., and van Duinen, R. J. 1980, *Ap. J.*, **241**, 173.
York, D. G., Blades, J. C., Cowie, L. L., Morton, D., Songaila, A., and Wu., C.-C. 1981, in preparation.

A. BOGGESS and T. R. GULL.: Code 683, Laboratory for Astronomy and Solar Physics, NASA, Goddard Space Flight Center, Greenbelt, MD 20771

C.-C. WU: Computer Sciences Corporation, Code 685, NASA, Goddard Space Flight Center, Greenbelt, MD 20771